Journal of Non-Newtonian Fluid Mechanics 301 (2022) 104751

Contents lists available at ScienceDirect

Journal of Non-Newtonian Fluid Mechanics

journal homepage: www.elsevier.com/locate/jnnfm

Shear-induced migration of a viscous drop in a viscoelastic liquid near a wall at high viscosity ratio: Reverse migration

Swarnajay Mukherjee [a], Anik Tarafder [b], Abhilash Reddy Malipeddi [b], Kausik Sarkar [b,*]

[a] Department of Mechanical Engineering, University of Delaware, United States
[b] Department of Mechanical and Aerospace Engineering, George Washington University, United States

ARTICLE INFO

Keywords:
Drop
Migration
Viscoelastic
FENE
Computational
Emulsion

ABSTRACT

Wall-induced migration of a viscous drop in a viscoelastic fluid subjected to a plane shear is numerically simulated to investigate the effects of drop/matrix viscosity ratio. In a Newtonian system, drop migration away from the wall is inhibited as the viscosity ratio is increased. Here, we show that the introduction of the matrix viscoelasticity further decreases the migration and can even reverse its direction 'from away' to 'towards the wall', a phenomenon not seen in Newtonian systems. The migration towards or away from the wall eventually settles in a quasi-steady state that only depends on the instantaneous wall separation independent of the initial position of the drop. Drops migrating towards the wall initially increase their velocity, but as they approach the wall, they decelerate, showing a non-monotonic variation. The migration direction depends on the viscosity ratio, viscoelasticity (Deborah number), and the capillary number. We compute phase diagrams in the parameter space showing boundaries where migration changes direction. The critical Deborah number (at a fixed viscosity ratio) and the critical viscosity ratio (at a fixed Deborah number) for direction reversal approximately scales with the inverse of the capillary number.

1. Introduction

The motion of drops and particles plays a critical role in many industrial applications such as food and polymer processing as well as in biological flows [1, 2, 3, 4]. It can give rise to an inhomogeneous distribution of fillers in processed polymeric parts [5] and a cell-free layer close to the wall in blood vessels [6, 7, 8]. Recent developments in microfluidics have led to renewed interest in particle and cell migration studies where inertia, viscoelasticity, confinement, and particle size individually or jointly could influence, and therefore could be manipulated to result in desired paths of suspended particles in the flow channel [9, 10, 11, 12, 13, 14]. Although migration of rigid particles in viscoelastic medium has received much attention, the literature is meager for viscoelastic effects on drop migration [3]. Drop deformability can introduce lateral migration even in inertialess Newtonian flow [15, 16, 17]. Deformability of particles can promote migration away from the wall in both viscous and viscoelastic medium where the latter seemed to reduce migration velocity and the migration velocity scales with the inverse square of instantaneous separation from wall [18]. Here, we extend our previous study of a viscosity-matched system to a high viscosity ratio system.

Migration of a single particle in simple flow conditions can provide great insight into the physics of fluid suspension and help to design efficient active or passive cell sorting/particle focusing microfluidic devices [19, 20, 21, 22, 23]. It is well known that in absence of inertia, reversibility of Stokes flow prevents any lateral motion of a neutrally buoyant rigid sphere in a shear flow near a wall [24, 25, 26]. Reversibility is broken by any one of several factors such as particle deformability, viscoelasticity or inertia. Numerous studies have been devoted to the investigation of lateral migration of drops, capsules and particles in shear (see [27] for a review of the literature before 1980). Effects of viscoelasticity on migration, especially for rigid particles, as noted before have also been investigated by various groups [9, 10, 28, 29, 30, 31, 32, 33, 34]. However, drop migration in presence of viscoelasticity has received very little attention [31].

Readers are referred to our previous article [18] for a detailed discussion of the migration literature. As noted above, the literature is extremely meager for viscoelastic effects on drop migration. There has only been a perturbative study in the limit of small deformation using a second-order fluid model [31]; it predicted that drop migration is

* Corresponding author at: Department of Mechanical and Aerospace Engineering, George Washington University, 800 22nd Street NW, Suite 3000, Washington, DC 20052, United States
E-mail address: Sarkar@gwu.edu (K. Sarkar).

https://doi.org/10.1016/j.jnnfm.2022.104751
Received 5 October 2021; Received in revised form 24 November 2021; Accepted 11 January 2022
Available online 14 January 2022

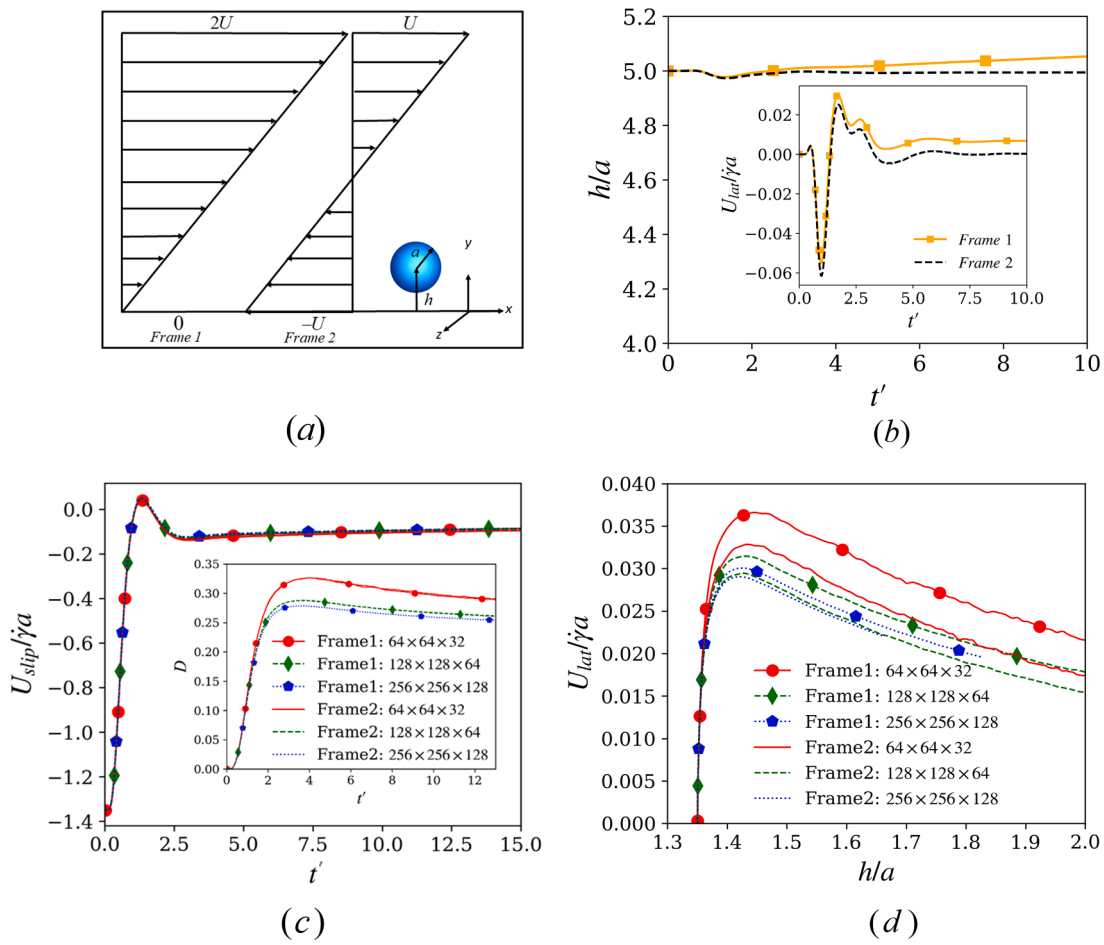

Fig. 1. (a) Schematic of the problem in two reference frames, (b) Drop position and migration velocity (inset) in two reference frames for *Ca=0.2, De=0.5,* $\lambda_\mu = 10$ (initially placed at the center of the domain ($h_i/a = 5.0$, equidistance from both the walls). (c) Slip velocity, drop deformation (inset) and (d) migration velocity of a viscous drop in a viscoelastic fluid for three grid resolutions in two reference frames for *Ca=0.2, De=0.5,* $\lambda_\mu = 1.0$ and initial position $h_i/a = 1.35$.

promoted by both drop and matrix phase viscoelasticity. Viscoelastic effects are often subtle and defy intuition, which is largely formed by our understanding of Newtonian fluid mechanics. The viscoelastic literature is fraught with contradictory findings—e.g. whether viscoelasticity increases or decreases drop deformation in free shear [35, 36, 37, 38]—along with no standard viscoelastic constitutive equation. For particle migration, the reasoning advanced is often physical and heuristic as in the case of a sphere in a shear flow between parallel plates, where the difference of the viscoelastic forces on the upper and the lower hemispheres was estimated to cause the lateral migration velocity with a cubic dependence on the blockage ratio of the particle [9, 34]. A similar theory balancing the drag force on a sphere with the viscoelastic force arising from the first normal stress difference varying with the local shear rate was used to explain the viscoelastic focusing seen in a microfluidic experiment with a polyvinyl pyrrolidone solution [11] as well as in a dilute DNA solution [21]. The deformable drop, as we noted before, introduces additional considerations. The situation demands careful analysis of canonical problems such as single drop migration with the simplest possible constitutive equations to help us understand the underlying physics.

The drop migration, we showed, is caused by the velocity induced by a stresslet field created by the drop in presence of the wall [39]. In our previous article, we gave a detailed derivation of the stresslet-induced migration velocity using a Green's function formulation including the viscoelastic contribution [18]. It clearly showed that the migration velocity arises from three different effects—an interfacial contribution, a viscoelastic contribution, and a third contribution arising from non-unity viscosity ratio—the first of the three pushing drops away from the wall and the latter two pulling towards the wall. For the viscosity matched system, in the range of Deborah numbers investigated, although viscoelasticity hindered lateral migration away from the wall, it did not change the migration direction. Here, we lift the restriction on the viscosity ratio. We would show that a high enough ratio of the drop to the matrix viscosity can reverse the migration direction to towards the wall. Also note that for a Newtonian system, a BEM simulation [40] showed that the migration velocity of a drop for a high enough viscosity ratio displays a significant deviation from the analytical expressions obtained using a perturbation method [31]. Such considerations amply justify the present study.

As in [18], we use a front tracking finite difference method and employ a modified version of the finitely extensible nonlinear elastic model due to Chilcott and Rallison (FENE-MCR) [41]. The model has one relaxation time, a constant shear viscosity and a positive first normal stress difference—all characteristics of a Boger fluid—and has been used in many viscoelastic studies[42, 43, 44, 45, 46]. The mathematical formulation and its numerical implementation are described in Section 2. Section 3 presents and discusses the results of the simulation, followed by conclusion in Section 4.

2. Mathematical formulation and numerical implementation

The mathematical formulation underlying our computational tool for simulating drops with viscoelastic constitutive equations has been described in our recent publication [18]. The complete droplet matrix

system is governed by the incompressible momentum conservation equations:

$$\frac{\partial(\rho\mathbf{u})}{\partial t} + \nabla\cdot(\rho\boldsymbol{uu}) = \nabla\cdot\tau - \int_{\partial B} d\mathrm{x_B}\kappa\mathbf{n}\Gamma\delta(\mathbf{x}-\mathbf{x_B}), \tag{1}$$

$$\nabla\cdot\mathbf{u} = 0 \tag{2}$$

in the entire domain Ω. The total stress $\boldsymbol{\tau}$ is decomposed into pressure, polymeric and viscous parts:

$$\boldsymbol{\tau} = -p\mathbf{I} + \mathbf{T}^p + \mathbf{T}^v,\ \mathbf{T}^v = \mu_s\mathbf{D}, \tag{3}$$

where p is the pressure, μ_s is the solvent viscosity, and $\mathbf{D} = (\nabla\mathbf{u}) + (\nabla\mathbf{u})^T$ is twice the strain rate tensor. The superscript T represents the transpose. $\boldsymbol{T}^p$ is the extra stress (or viscoelastic stress) due to the presence of polymer. In Eq. (1) Γ is the interfacial tension (constant), ∂B represents the surface of the drop consisting of points $\mathbf{x}_B$, κ the local curvature, $\mathbf{n}$ the outward normal, and $\delta(\mathbf{x}-\mathbf{x}_B)$ is the three-dimensional Dirac delta function. The FENE-CR constitutive equation in terms of the conformation tensor $\mathbf{A}$ is given by [41] (see a detailed discussion of the method and its use in [18]):

$$\frac{\partial\mathbf{A}}{\partial t} + \mathbf{u}\cdot\nabla\mathbf{A} = \nabla\mathbf{u}\cdot\mathbf{A} + \mathbf{A}\cdot(\nabla\mathbf{u})^T - \frac{f}{\lambda}(\mathbf{A}-\mathrm{I})\ where\ f = \frac{L^2}{L^2 - tr(\mathbf{A})} \tag{4}$$

The relation between the stress $\mathbf{T}^p$ and conformation tensor $\mathbf{A}$is:

$$\mathbf{A} = \left(\frac{\lambda}{\mu_p f}\right)\mathbf{T}^p + \mathbf{I} \tag{5}$$

Therefore, the stress constitutive equation becomes:

$$\frac{\partial\mathbf{T}^p}{\partial t} + \left\{\mathbf{u}\cdot\nabla\mathbf{T}^p - \nabla\mathbf{u}\cdot\mathbf{T}^p - \mathbf{T}^p\cdot\nabla\mathbf{u}^T\right\} + f\mathbf{T}^p\left[\frac{\partial}{\partial t}(1/f) + \mathbf{u}\cdot\nabla(1/f)\right] + \frac{f}{\lambda}\mathbf{T}^p = \frac{f}{\lambda}\mu_p\mathbf{D}. \tag{6}$$

$$where\ f = \frac{L^2 + \lambda/\mu_p(\sum T^p_{ii})}{L^2 - 3}, \tag{7}$$

μ_p is the polymeric viscosity, λ is the relaxation time, and L is the finite extensibility. FENE-CR model introduces finite extensibility limiting the maximum length of the end-to-end vector for the polymer molecule. In the limit of $L\to\infty$ we obtain the Oldroyd-B equation. The terms $f\mathbf{T}^p\left[\frac{\partial}{\partial t}(1/f) + \mathbf{u}\cdot\nabla(1/f)\right]$ are negligible in our simulations, and by dropping them we arrive at the FENE-MCR equation:

$$\frac{\partial\mathbf{T}^p}{\partial t} + \left\{\mathbf{u}\cdot\nabla\mathbf{T}^p - \nabla\mathbf{u}\cdot\mathbf{T}^p - \mathbf{T}^p\cdot\nabla\mathbf{u}^T\right\} + \frac{f}{\lambda}\mathbf{T}^p = \frac{f}{\lambda}\mu_p\mathbf{D}. \tag{8}$$

By using an elastic and viscous stress splitting method used by [47], the viscoelastic stress can be expressed in the following form:

$$(\mathbf{T}^p)^{n+1} = \left[(\mathbf{T}^p)^n - (\mu_p\mathbf{D})^n\right]e^{-(f/\lambda)\Delta t} + (\mu_p\mathbf{D})^n - \frac{\lambda}{f}\left[\mathbf{u}\cdot\nabla\mathbf{T}^p - \nabla\mathbf{u}\cdot\mathbf{T}^p - \mathbf{T}^p\cdot\nabla\mathbf{u}^T\right]^n\left[1 - e^{-(f/\lambda)\Delta t}\right]. \tag{9}$$

A spherical drop of radius a is placed in a computational domain at $t = 0$ in close proximity—distance h_i—to the bottom wall (equidistant from the side boundaries) (Fig.1a frame 2). Although the problem of interest is a simple shear flow near a wall, computationally one needs a finite computational domain of sufficiently large dimensions with conditions imposed on the boundaries to simulate the shear flow. We choose the size to be $L_x = 10a$, $L_y = 10a$ and $L_z = 5a$ in the flow, gradient and the vorticity directions, which was shown to be sufficient in our previous investigations [15, 18, 48]. The upper plate (y-direction domain boundary) is impulsively started (in the x–direction) with a velocity U and the lower plate with a velocity -U at $t = 0$ creating a shear rate of $\dot{\gamma} = 2U/L_y$. Periodic conditions are imposed in the flow and the vorticity directions. The drop is described by a triangulated front distinct from the regular Cartesian grid used to solve the flow field; the front is adaptively regridded to prevent excessive distortion of the front elements. A multigrid method is used for the pressure Poisson equation, and an ADI method is used to alleviate the diffusion restriction on the time step. Other details can be found in previous papers [47, 49, 50, 51, 52, 53, 54]. We use a and $\dot{\gamma}^{-1}$ for non-dimensionalizing length and time scales respectively (with $t' = t\dot{\gamma}$). The dimensionless parameters are Reynolds number $\mathrm{Re} = \rho_m a^2\dot{\gamma}/\mu_m$ capillary number $Ca = \mu_m a\dot{\gamma}/\Gamma$, Deborah number $De = \lambda\dot{\gamma}$ (which for the present purpose is similar to the Weissenberg number), viscosity ratio $\lambda_\mu = \mu_d/\mu_m$, density ratio $\lambda_\rho = \rho_d/\rho_m$ and $\beta = \mu_{pm}/\mu_m$—the ratio of the polymeric to the total drop viscosity. Additionally, the initial condition is characterized by the nondimensional drop-wall separation h_i/a. In the matrix, the viscosity is $\mu_m = \mu_{sm} + \mu_{pm}$, the sum of the solvent and polymeric viscosities. In all of our simulations, the density ratio has been kept fixed at a value of unity. We have chosen $\beta = 0.9$ and $L = 20$. In our previous study of the viscosity matched case, we found that the migration velocity become insensitive to L above this value [18]. Effects of β variation have been investigated in detail for the viscosity-matched system to show that the viscoelastic effects are largely governed by the product βDe [18]. The explicit nature of the code restricts us (despite the ADI implementation of the viscous terms) to a small non-zero Reynolds number which is kept at a value of 0.03 where inertial effects are negligible. Effects of the top wall (a numerical artifact) were investigated to find that for $h/a < 3.5$ dynamics remain independent of the top wall. Convergence of the viscoelastic algorithm used to simulate fluids with Oldroyd-B constitutive relation has been established for a number of drop dynamic problems—deformation in shear flows [37, 38, 55], high viscosity ratio system [56], drop retraction [57] and sedimentation in quiescent fluid [58]. For the FENE-MCR relation, grid independence was investigated for shear induced drop migration in our previous paper [18]. In this study, we choose 128 × 128 × 64 discretization in the flow, gradient and vorticity directions (the effects of discretization is briefly discussed below).

We note that in our previous studies [15, 18, 48], we imposed an impulsively started velocity 2U on the upper (y-directional) boundary and a zero velocity on the lower one to create the shear flow with the same rate $\dot{\gamma} = 2U/L_y$ (Fig. 1a, frame 1). The two flows (frames 1 and 2) are equivalent under Galilean transformation, and therefore the physics remains the same in both (representing two different reference frames). However, note that numerically the drop shapes and motion are

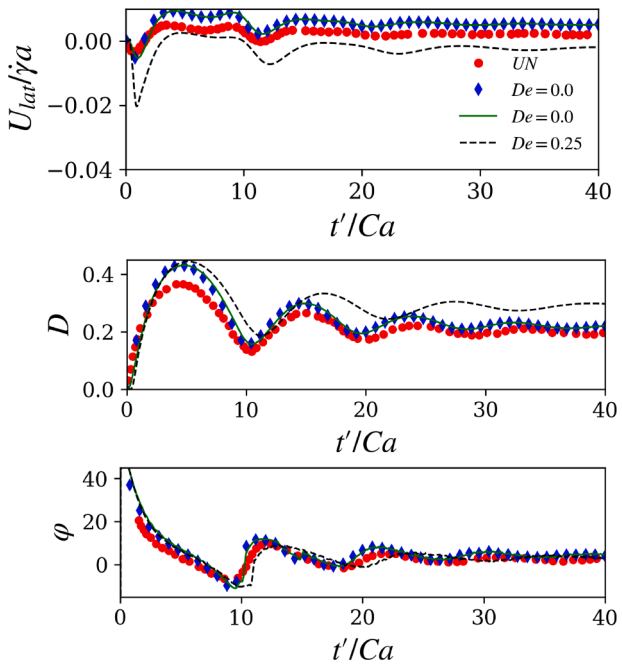

Fig. 2. Lateral velocity, deformation and orientation angle for $Ca = 1.5$, $\lambda_\mu = 10$, and $h_i/a = 1.5$ are compared with BEM simulations of Uijttewaaal and Nijhof (UN). Dotted curves in color blue (our simulation) and red (BEM) are computed with initially fully developed shear for the viscous case ($De = 0$). The other two curves are with impulsively started flow for De =0 (solid) and De = 0.25 (dash).

determined by the movement of the mesh points on the front using velocity interpolated from the 3D Cartesian grid, and therefore they are prone to numerical error of the particular discretization level. Such grid related issues resulting in the sensitivity of particle trajectory were also observed in finite element simulations of deformable particles in a channel flow [16], where a particle placed initially at the diagonal of a square cross-section didn't exactly follow the diagonal line of the cross-section during lateral movement. Our choice in favor of the symmetric flow (frame 2 in Fig. 1a) is dictated by a numerical investigation of the results in two reference frames (Fig. 1). In Fig. 1(b), we see that a drop placed at the center of the domain, therefore expected to not move, shows a very small fluctuating initial lateral velocity, due to the drop deformation and initial adjustment. However, eventually, only the flow in symmetric frame 2 leads to a zero velocity preserving the imposed symmetry of the computational flow. The one in the asymmetric frame leads to small but finite positive lateral velocity. For the physical flow of interest here, the computational domain, as noted, is only a numerical artifact, and therefore the centerline is not of any significance. However, such numerical errors are to be avoided if possible. We also investigate a drop in close proximity to the lower boundary and compute the flow in two different reference frames at different discretization levels 64 × 64 × 32, 128 × 128 × 64 and 256 × 256 × 128. In Fig. 1(c), the slip velocity (measured relative to the local shear velocity) and deformation (in the inset) plotted for the two reference frames don't differ at the same discretization, both reducing with increased discretization. However, in Fig. 1(d), we note that although results in both reference frames eventually converge with increasing discretization, frame 2 converges faster. We therefore choose frame 2 with 128 × 128 × 64 discretization.

3. Results

In our recent study of a viscosity-matched system [18], we developed a theory of drop migration using Stokes Green's function to show that the migration velocity is determined by the image stresslet field induced by the drop because of the presence of the wall. Accordingly, far from the wall, the migration velocity can be written as

$$U_{lat} = -\frac{1}{8\pi\mu_m}\left(\frac{9}{8h^2}\right)\left(S_{22}^{\text{int}} + S_{22}^{\text{vrat}} + S_{22}^{NN}\right), \tag{10}$$

where three different stresslet terms are 1) interfacial stresslet S_{22}^{int} arising from interfacial tension acting at the drop interface, a purely geometric term determined by the drop shape, 2) S_{22}^{vrat} arising due to non-unity viscosity ratio, and 3) S_{22}^{NN} arising from viscoelastic stresses around the drop (definitions of the S_{22}'s are given in [18]). The matrix viscoelasticity affects the migration in two competing ways. It decreases the drop inclination angle thereby increasing the interfacial contribution aiding migration, which however is outweighed by the direct inhibitory effect of the viscoelastic stresses resulting in a net reduction in migration velocity. From the theory, it is clear that the second term due to the viscosity ratio also inhibits migration at large viscosity ratios. Here, we investigate this effect of the viscosity ratio. Due to the rather small drop-wall distances considered here, the stresslet-based theory developed in [18] is not valid and therefore cannot be used for quantitative comparison. However, it helps us understand the results.

3.1. Comparison with BEM solution and effects of Deborah number

In our previous paper [18], we showed a very good comparison between our results—drop deformation and migration velocity for the Newtonian system of a viscosity matched drop in a wall-bounded shear—with those from BEM simulations [59] and theoretical expressions of Chan and Leal [31] and Shapira and Haber [60]. In Fig.2 we consider the case of a high viscosity ratio of $\lambda_\mu = 10$ at Ca=1.5 and $h_i/a = 1.5$. We first consider a Newtonian case ($De = 0$) and compare the time evolution of lateral velocity, deformation and orientation angle with BEM simulation [40]. We use nondimensional time $t'/Ca = t\Gamma/\mu_m a$ of the BEM article. The deformation shows oscillations and wobbly motion as is typical for high viscosity ratio drops. The inclination angle oscillates, but eventually decreases away from the extension axis of the shear at $\pi/4$ to align with the flow. The deformation and the inclination angle show excellent match between the two independent computations except at the initial period. The small discrepancy (between the blue and the red dotted curved) is due to the finite inertia ($Re = 0.03$) in our computation. However, they all show the same details of time-variation (magnitude and periodicity) albeit with slight variation in magnitudes, especially for the velocity. Note that unlike in BEM computation of Stokes flow, due to the finite inertia in our computation, it takes a finite time for the shear to establish after the impulsive start of the top boundary. For comparison with the BEM simulation, we have used a fully developed linear shear flow as the initial velocity field as opposed to fluid initially at rest impulsively started by the top and the bottom boundaries as in all other computations in the paper.

In the same figure, we include a viscoelastic case—$De = 0.25$. Viscoelasticity increases deformation, changes inclination, and retards migration velocity. For $De = 0.25$, the velocity is negative and the drop moves towards the wall. Both higher viscosity ratio and viscoelasticity retard migration, but in combination, they here reverse the direction of migration. For the viscosity matched cases, within the range of Deborah numbers considered [18], we did not observe such a reversal. However, rigid spheres—which is retrieved for a drop in the limit of $\lambda_\mu \to \infty$—were shown to migrate towards the closest wall in a shear flow [61].

In Fig. 3(a), we plot the evolution of the dimensionless distance of the drop from the wall for varying De at $Ca = 0.2$, $\lambda_\mu = 10$, and $h_i/a = 1.5$. With increasing viscoelasticity, the migration away from the wall gets retarded, and eventually reverses its direction to towards the wall at De= 0.5. Fig. 3(b) shows the same by plotting the migration velocity as a function of time. With increasing De, the drop is pulled more towards the wall. When the viscoelastic contribution can overcome the combined effect of interfacial and viscous stresses, the drop migrates towards the wall. Fig. 3(c) plots drop deformation and the angle of inclination as a

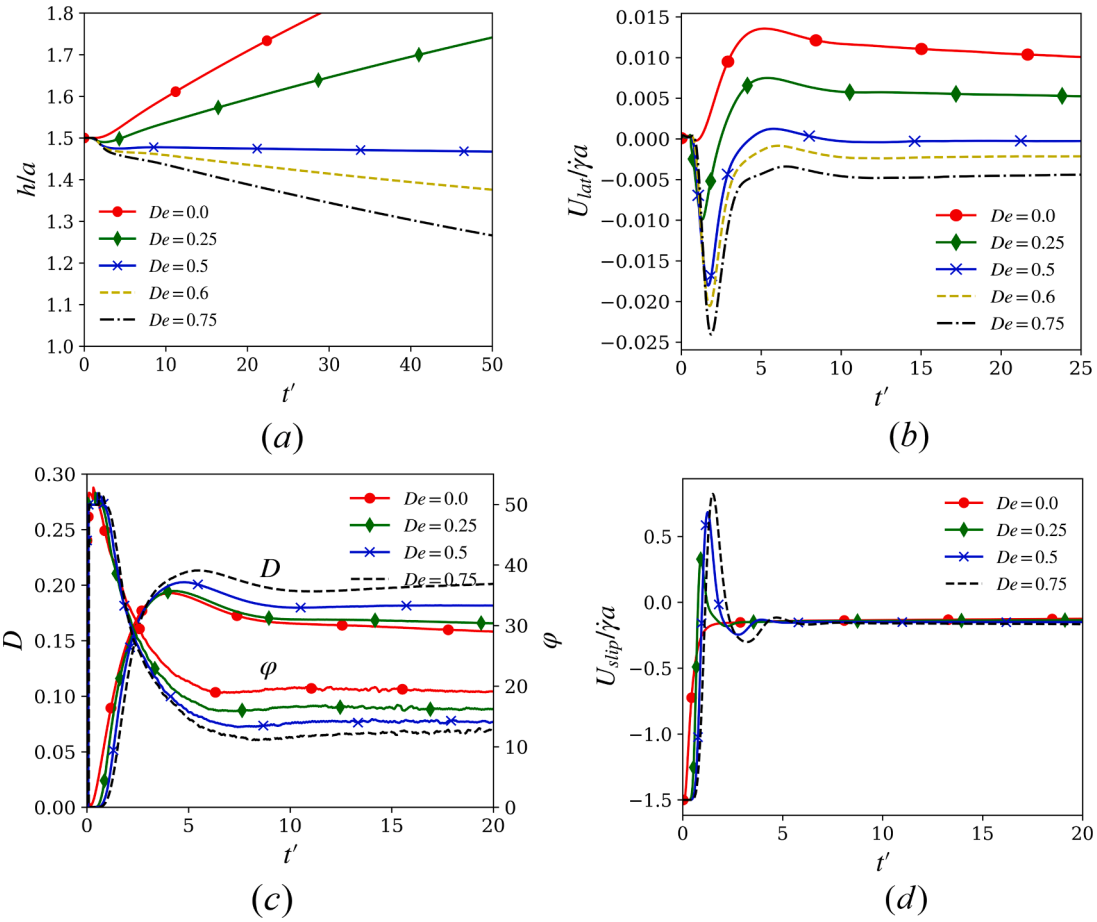

Fig. 3. Drop migration for varying *De* for $Ca = 0.2$, $\lambda_\mu = 10$ and $h_i/a = 1.5$: (a) Drop height , (b) lateral migration velocity, (c) deformation and inclination angle, and (d) slip velocity.

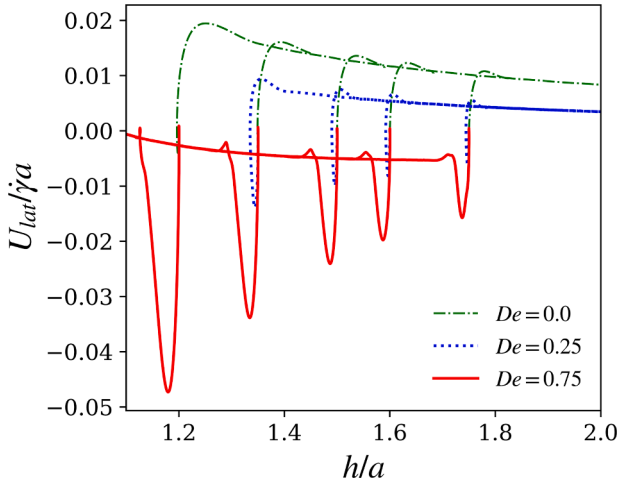

Fig. 4. Lateral migration velocity as a function of the distance from the wall for Newtonian and viscoelastic cases for $Ca = 0.2$, $\lambda_\mu = 10$ and varying *De*.

function of time for different *De* with other parameters kept the same. The deformation increases with increasing viscoelasticity due to viscoelastic stretching as well as the drop being nearer to the wall experiences a higher local strain rate. Previous numerical studies described the importance of inclination angle in migration [40]. At this high $\lambda_\mu = 10$, the inclination angle even for a Newtonian case is quite small, 19°. The decrease in angle with increasing Deborah number considered here is not too large (12°∼16°). Slip velocities (Fig. 3d) show that during the transient phase, there is an overshoot and for higher *De*, the value can become positive i.e., the drop leads the flow. This is only temporary, and a quasi-steady state is reached where slip velocities are negative and do not vary significantly with Deborah number. The drop deformation is computed from the farthest and the nearest points on the drop interface, which in turn is evolved by velocities interpolated on the front vertices from the field in the Eulerian grid. This numerical procedure gives rise to the slight lack of smoothness seen in some of the curves in Fig. 3(c) and in other figures below.

In Fig. 4, we investigate lateral migration as a function of separation from the wall with drops initially placed at different initial heights from the wall. Three cases, $De = 0$, 0.25 and 0.75 are considered. As we saw in the viscosity matched system, the curves for different initial heights eventually collapse on each other indicating quasi-steady dynamics independent of the initial condition. For the Newtonian and the $De = 0.25$ cases, the quasi-steady velocities are positive. However, for $De = 0.75$, the drop has a negative velocity. For the latter case, as the drop approaches the wall, around $h/a = 1.1$, the velocity almost reaches zero. The transients are different in the three cases. For the Newtonian and $De = 0.25$, the velocity initially increases and then settles down as the quasi-steady state is reached. For $De = 0.75$, the curve looks similar except that the velocity, as mentioned, remains negative.

3.2. *Effects of viscosity ratio and capillary number*

Increasing the viscosity ratio λ_μ has two well-known effects on the drop geometry—the deformation decreases and the drop gets increasingly aligned with the flow. In Fig. 5(a), we plot the evolution of drop

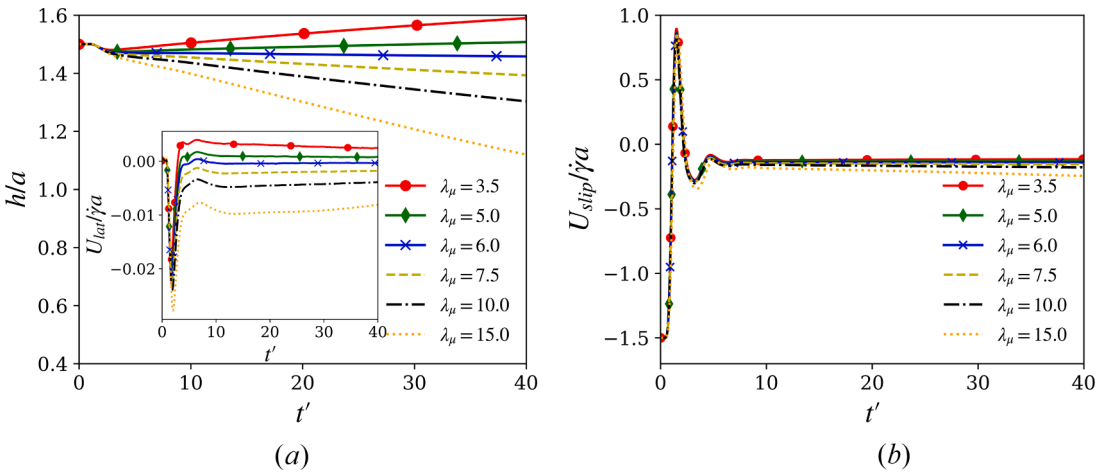

Fig. 5. (a) Non-dimensional height vs. time for $Ca = 0.2$, $De = 0.75$, and $h_i/a = 1.5$. The inset shows the time variation of lateral velocity. (b) Time evolution of slip velocity for the same parameters.

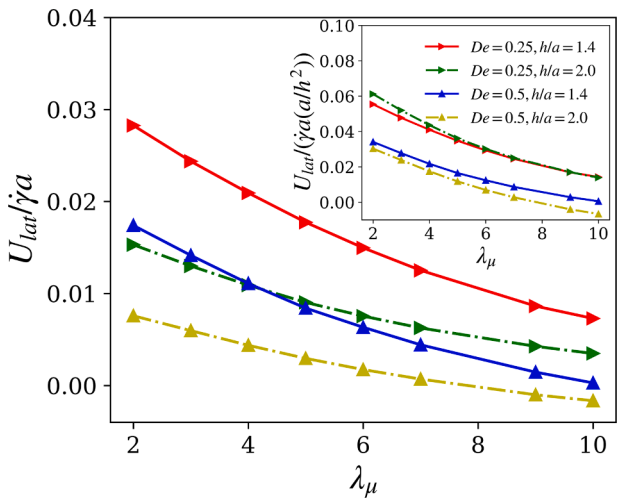

Fig. 6. Quasi-steady migration velocity as a function of viscosity ratio, at two different Deborah numbers and h/a (legends are same as in the inset) for $Ca = 0.2$. Inset shows the same scaled by $(a/h)^2$.

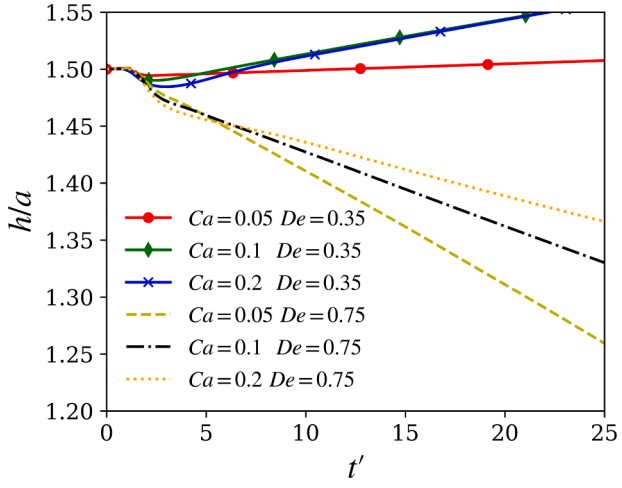

Fig. 7. Evolution of the non-dimensional drop height for different capillary and Deborah numbers and $\lambda_\mu = 10$.

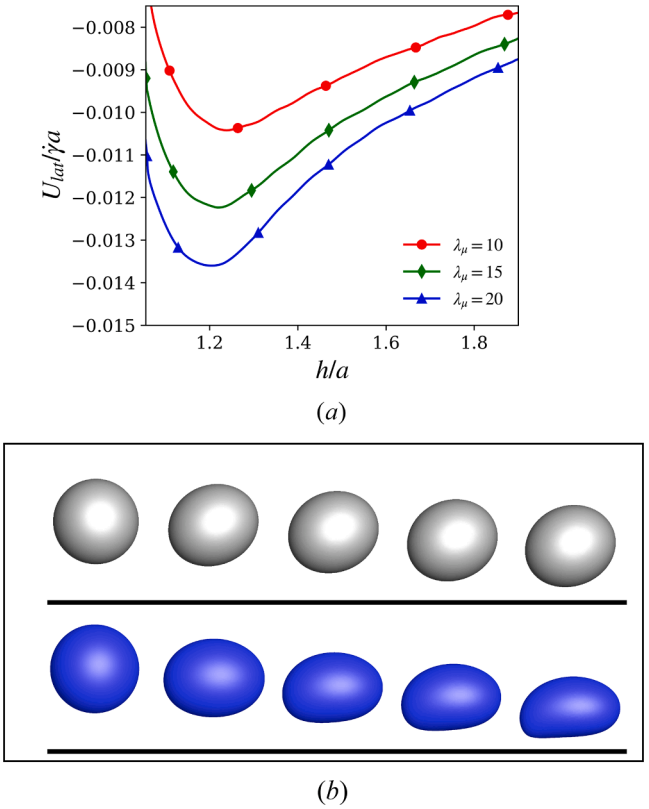

Fig. 8. (a) Quasi-steady velocities plotted vs. drop height for $Ca = 0.05$ and $De = 0.75$ for different viscosity ratios. (b) Shapes of drops (horizontal position is arbitrary) migrating towards the wall (black line) at successive time instants for $De = 0.75$, $Ca = 0.05$, $h_i/a = 1.5$,$\lambda_\mu = 10$ (top) and $De = 0.75$, $Ca = 0.2$, $h_i/a = 1.5$, $\lambda_\mu = 20$ (bottom).

height for $Ca = 0.2$, $De = 0.75$ and $h_i/a = 1.5$ with varying viscosity ratios. The drop initially experiences a negative migration velocity for all λ_μ (seen clearly in the inset) moving towards the wall but later they settle either for migration away from the wall for $\lambda_\mu < 6.0$, or towards the wall for larger $\lambda_\mu > 6.0$. Fig. 5(b) shows very little effects of viscosity ratio on slip velocity evolution.

Fig. 6 plots the lateral velocity as a function of λ_μ (in the quasi-steady state) for Ca=0.2 and two Deborah numbers. For a particular height, the curves for two De are almost parallel to each other. Given the analytical

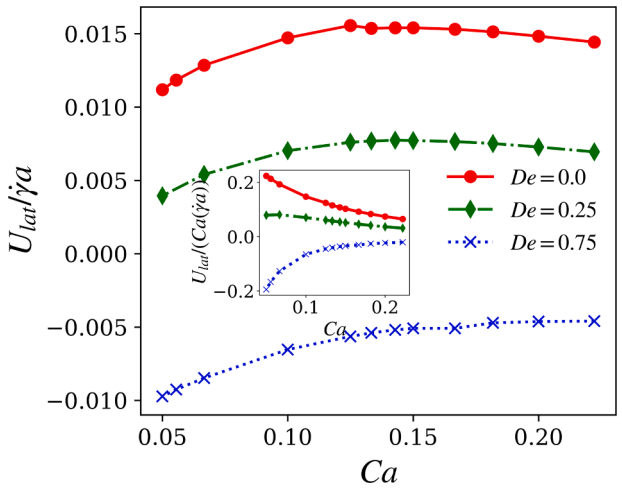

Fig. 9. Lateral migration velocities plotted for $\lambda_\mu = 10$ and at instantaneous height of $1.4a$ to show Capillary variation of lateral velocities for different Deborah numbers. Inset shows the lateral velocities divided by Ca.

theory [18, 31] that predicts $U_{lat}/\dot{\gamma}a \sim Ca(a/h)^2$, in the inset we plot $U_{lat}(a/h)^2/\dot{\gamma}a$ to show that the scaling is only approximate (as was also seen in the viscosity matched system [18]). For a Newtonian case, Uijttewaaal and Nijhof [40] also observed that the scaling does not hold exactly except at small Ca ∼0.1 and large wall separation h/a ∼20. Increasing capillary number increases drop deformation promoting migration away from the wall. Increasing matrix viscoelasticity pushes the drop towards the wall reducing the validity of the scaling law.

In Fig. 7, we plot the time evolution of drop heights for three different capillary numbers and two Deborah numbers at $\lambda_\mu = 10$. At the lower Deborah number $De = 0.35$, the drop migrates away from the wall for $Ca = 0.2$, Ca =0.1 and $Ca = 0.05$, migration speed decreasing with decreasing Ca. At $De = 0.75$, the drop migrates towards the wall for all three Ca values, the absolute speed of migration increasing with decreasing Ca.

Fig. 8(a) plots migration velocity for $Ca = 0.05$, $De = 0.75$ and varying viscosity ratios, where the drop migrates towards the wall. As the drop approaches the wall, the absolute value of the velocity first increases, reaches a maximum, and then decreases. The maximum velocity magnitude increases with increasing viscosity ratio, with the location shifting slightly towards the wall. The velocity maximum can be explained by noting the following fact. The presence of the wall is the cause of drop migration; far away from the wall the wall-ward migration velocity is small and increases as the drop approaches the wall. However, the motion is finally impeded close to the wall, and the migration velocity has to eventually decrease to zero. Therefore, in its approach to the wall, the absolute velocity would pass through a maximum. The curves have been averaged to eliminate slight oscillations arising due to the numerical issues noted while describing Fig. 3(c) further aggravated by the numerical differentiation of the position to compute the velocity. At proximity to the wall, the drop shape is affected by the wall, lubrication forces in the small gap are strong, and the drop experiences strong deformation. Figs. 8(b) shows drop shapes and heights (but not correct x positions) at some consecutive times for two different viscosity ratios. The drop assumes flattened shapes effectively lowering the height of its center of mass.

In Fig. 9, we plot the migration velocity as a function of capillary number at an instantaneous height $h/a = 1.4$ for different De values. With increasing Ca, migration velocity initially increases, reaches a maximum and then slightly reduces. Note that the previous BEM simulation [40] also showed such nonmonotonicity at high viscosity ratios. The deviation from the analytic result $U_{lat}/\dot{\gamma}a \sim Ca(a/h)^2$ can be seen clearly in the inset where the migration velocity divided by capillary numbers is plotted. The viscoelastic curves follow a similar trend with velocity decreasing and eventually becoming negative with increasing De.

3.3. Phase diagrams for positive and negative migration

We have found that increasing viscoelasticity and viscosity ratio promotes migration towards the wall, whereas increasing capillary number pushes it away from the wall. The competition governs the dynamics and results in either a positive or a negative migration velocity for the drop. In this section, we present phase diagrams determining the regions in this parameter space for these two behaviors. Fig. 10(a) plots the phase diagram for Ca and λ_μ for drops initially positioned at $h_i/a =$ 1.5 and $De = 0.75$. Each symbol represents a simulation; upward triangles represent drops eventually going away from the wall and downward triangles represent moving towards the wall. As Ca is increased, a higher value of viscosity ratio is required to make the drop migrate down towards the wall. The color contour shows the migration velocity positive i.e., away from the wall for more deformable drops and low viscosity ratios, reducing velocity as viscosity ratio λ_μ is increased and Ca decreased, eventually reversing direction towards the wall. An approximate linear relation $\lambda_{\mu,critical} \sim Ca^{-1}$ is noticed between the inverse of capillary number and the viscosity ratio. Fig. 10(b) plots a similar phase diagram in De-Ca space for $h_i/a = 1.5$ and $\lambda_\mu = 10$. The drops above the green line (downward triangles) eventually migrate

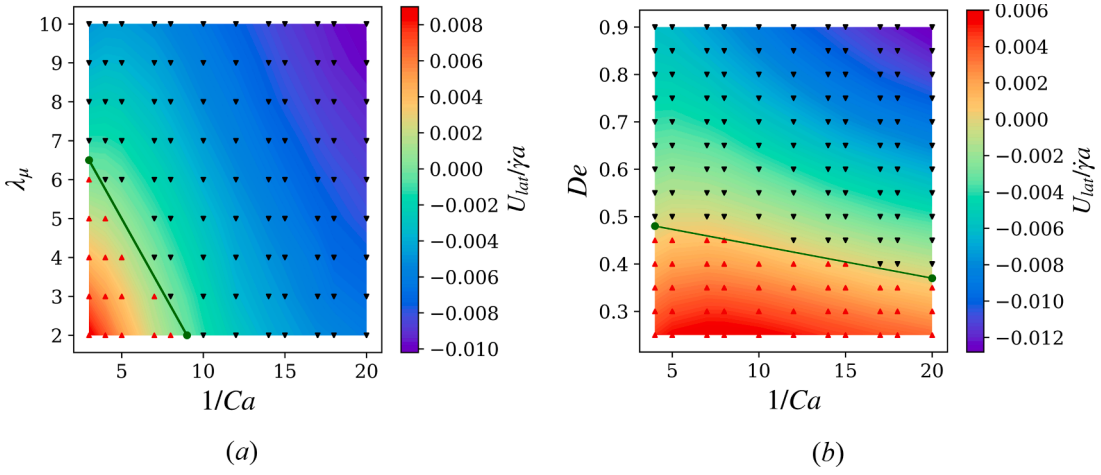

(a) (b)

Fig. 10. Phase diagrams for the direction of drop migration: (a) In λ_μ-Ca space for$De = 0.75$ and $h_i/a = 1.5$. (b) In De-Ca space for $\lambda_\mu = 10$, $h_i/a = 1.5$. Drops below the green lines migrate away from the wall and those above migrate towards the wall. The color contour describes the migration velocity.

towards the wall, and those below (upward triangles) migrate away from the wall, showing here also an approximately linear relation $De_{critical} \sim Ca^{-1}$. In both figures, away from the phase boundaries the velocity magnitudes increase. Note that the stresslet theory and the phenomenological relation for migration both predicted $U_{lat}/\dot{\gamma}a \sim (K_1 Ca - K_2 De - K_3 CaDe)$ [18]. Neglecting the third term for small Ca gives $De_{critical} \sim Ca^{-1}$ for zero migration velocity.

4. Conclusions

Following our recent numerical investigation of the migration of a viscosity-matched viscous drop in a viscoelastic matrix [18], in this paper, we investigate the same phenomenon for high drop to matrix viscosity ratios. Our earlier investigation showed that matrix viscoelasticity retards migration of a drop away from the wall—the effect stemming from the viscoelastic normal stresses along the curved streamlines around the drop. Here, we see that at high viscosity ratios, strong enough viscoelasticity can reverse the migration direction from away from the wall to towards the wall. The migration velocity eventually becomes quasi-steady depending only on its instantaneous separation from the wall. For drops migrating towards the wall, their approach velocity shows a non-monotonic variation with the distance from the wall. The slip velocity is briefly investigated to show that it is not a strong function of λ_μ.

We noted in our previous work, that the migration is caused by three distinct effects—an interfacial term, a viscosity ratio term and a viscoelastic term, the latter two inhibiting the migration away from the wall caused by the first one. The competition between the three determines the direction of the migration. With numerous simulations varying De, Ca and λ_μ, we obtain phase diagrams showing the critical values of parameters that distinguish migration direction towards or away from the wall. The critical parameters show approximate relations: $\lambda_{\mu,critical} \sim Ca^{-1}$ for a fixed De, and $De_{critical} \sim Ca^{-1}$ for a fixed λ_μ. Note that in an emulsion with multiple drops, migration along with shear-driven collision determines the final drop distribution—a phenomenon that has been studied for Newtonian systems [62, 63]. The wall-ward migration presented here indicates fundamentally different physics for viscoelastic emulsions and warrants further investigation.

Declaration of Competing Interest

The authors declare that they have no known competing financial interests or personal relationships that could have appeared to influence the work reported in this paper.

Acknowledgement

KS acknowledges partial financial support from NSF Grants No. CBET-0625599, CBET-0651912, CBET-1033256, DMR-1239105, CBET-1205322, and CMMI 2019507. Authors acknowledge time on the Pegasus cluster at GWU. KS thanks Professor Bill Schowalter for reading a draft and offering his insights. The computation was also performed using the Comet cluster at the San Diego Supercomputer Center, through the Extreme Science and Engineering Discovery Environment (XSEDE) program [64], which is supported by the National Science Foundation grant number ACI-1548562 (CTS180042).

References

[1] A.C. Barbati, et al., Complex fluids and hydraulic fracturing, Annu. Rev. Chem. Biomol. Eng. 7 (2016) 415–453.
[2] J.F. Morris, Toward a fluid mechanics of suspensions, Phys. Rev. Fluids 5 (11) (2020), 110519.
[3] A.H. Raffiee, S. Dabiri, A.M. Ardekani, Suspension of deformable particles in Newtonian and viscoelastic fluids in a microchannel, Microfluid. Nanofluidics 23 (2) (2019) 22.
[4] E.S. Shaqfeh, On the rheology of particle suspensions in viscoelastic fluids, AIChE J. 65 (5) (2019) e16575.
[5] R.P. Hegler, G. Mennig, Phase-separation effects in processing of glass-bead-filled and glass-fiber-filled thermoplastics by injection-molding, Polymer Eng. Sci. 25 (7) (1985) 395–405.
[6] J.H. Barbee, G.R. Cokelet, The fahraeus effect, Microvasc. Res. 3 (1) (1971) 6–16.
[7] R. Fåhraeus, The suspension stability of the blood, Physiol. Rev. 9 (2) (1929) 241–274.
[8] G.J. Tangelder, et al., Distribution of blood platelets flowing in arterioles, Am. J. Physiol.-Heart and Circulatory Physiol. 248 (3) (1985) H318–H323.
[9] G. D'Avino, F. Greco, P.L. Maffettone, Particle migration due to viscoelasticity of the suspending liquid and its relevance in microfluidic devices, Annu. Rev. Fluid Mech. 49 (2017) 341–360.
[10] J. Zhou, I. Papautsky, Viscoelastic microfluidics: progress and challenges, Microsyst. Nanoengineering 6 (1) (2020) 1–24.
[11] A.M. Leshansky, et al., Tunable nonlinear viscoelastic ``focusing'' in a microfluidic device, Phys. Rev. Lett. 98 (23) (2007), 234501.
[12] E.J. Lim, et al., Inertio-elastic focusing of bioparticles in microchannels at high throughput, Nat. Commun. 5 (1) (2014) 4120.
[13] K. Sarkar, R.K. Singh, Spatial ordering due to hydrodynamic interactions between a pair of colliding drops in a confined shear, Phys. Fluids 25 (5) (2013).
[14] S. Singha, et al., Mechanisms of spontaneous chain formation and subsequent microstructural evolution in shear-driven strongly confined drop monolayers, Soft Matter 15 (24) (2019) 4873–4889.
[15] R.K. Singh, X.Y. Li, K. Sarkar, Lateral migration of a capsule in plane shear near a wall, J. Fluid Mech. 739 (2014) 421–443.
[16] M.M. Villone, Lateral migration of deformable particles in microfluidic channel flow of Newtonian and viscoelastic media: a computational study, Microfluid. Nanofluidics 23 (3) (2019) 1–13.
[17] M.M. Villone, et al., Numerical simulations of deformable particle lateral migration in tube flow of Newtonian and viscoelastic media, J. Nonnewton Fluid Mech. 234 (2016) 105–113.
[18] S. Mukherjee, K. Sarkar, Effects of matrix viscoelasticity on the lateral migration of a deformable drop in a wall-bounded shear, J. Fluid Mech. 727 (2013) 318–345.
[19] A.A.S. Bhagat, S.S. Kuntaegowdanahalli, I. Papautsky, Inertial microfluidics for continuous particle filtration and extraction, Microfluid. Nanofluidics 7 (2) (2009) 217–226.
[20] D.W. Inglis, et al., Critical particle size for fractionation by deterministic lateral displacement, Lab on a Chip, 6 (5) (2006) 655–658.
[21] K. Kang, et al., DNA-based highly tunable particle focuser, Nat. Commun. 4 (1) (2013) 2567.
[22] S. Yang, et al., Sheathless elasto-inertial particle focusing and continuous separation in a straight rectangular microchannel, Lab on a Chip, 11 (2) (2011) 266–273.
[23] H.A. Nieuwstadt, et al., Microfluidic particle sorting utilizing inertial lift force, Biomed. Microdevices 13 (1) (2011) 97–105.
[24] P.G. Saffman, On the motion of small spheroidal particles in a viscous liquid, J. Fluid Mech. 1 (05) (1956) 540–553.
[25] F.P. Bretherton, The motion of rigid particles in a shear flow at low Reynolds number, J. Fluid Mech. 14 (2) (1962) 284–304.
[26] L.G. Leal, Advanced Transport Phenomena: Fluid Mechanics and Convective Transport, Cambridge University Press, New York, 2007.
[27] L.G. Leal, Particle motions in a viscous fluid, Annu. Rev. Fluid Mech. 12 (1) (1980) 435–476.
[28] A. Karnis, S.G. Mason, Particle motions in sheared suspensions, XIX. Viscoelastic Media. Trans. Society of Rheol. 10 (2) (1966) 571–592.
[29] E. Bartram, H.L. Goldsmith, S.G. Mason, Particle motions in non-newtonian media III. Further observations in elasticoviscous fluids, Rhelogical Acta 14 (9) (1975) 776–782.
[30] B.P. Ho, L.G. Leal, Migration of rigid spheres in a 2-dimensional unidirectional shear-flow of a 2nd-order fluid, J. Fluid Mech. 76 (Aug25) (1976) 783–799.
[31] P.C.H. Chan, L.G. Leal, The motion of a deformable drop in a second-order fluid, J. Fluid Mech. 92 (01) (1979) 131–170.
[32] J. Feng, D.D. Joseph, The motion of solid particles suspended in viscoelastic liquids under torsional shear, J. Fluid Mech. 324 (1996) 199–222.
[33] P.Y. Huang, et al., Direct simulation of the motion of solid particles in Couette and Poiseuille flows of viscoelastic fluids, J. Fluid Mech. 343 (1997) 73–94.
[34] G. D'Avino, et al., Viscoelasticity-induced migration of a rigid sphere in confined shear flow, J. Nonnewton Fluid Mech. 165 (9–10) (2010) 466.
[35] T. Tavgac, Ph.D Thesis (Chemical Engineering), Univ. of Houston, Texas, 1972.
[36] J.J. Elmendorp, R.J. Maalcke, A study on polymer blending microrheology. 1, Polymer Engng. Sci. 25 (1985) 1041–1047.
[37] N. Aggarwal, K. Sarkar, Deformation and breakup of a viscoelastic drop in a Newtonian matrix under steady shear, J. Fluid Mech. 584 (2007) 1–21.
[38] N. Aggarwal, K. Sarkar, Effects of matrix viscoelasticity on viscous and viscoelastic drop deformation in a shear flow, J. Fluid Mech. 601 (2008) 63–84.
[39] J.R. Smart, D.T. Leighton Jr., Measurement of the drift of a droplet due to the presence of a plane, Phys. Fluids A: Fluid Dynamics 3 (1) (1991) 21–28.
[40] W.S.J. Uijttewaal, E.J. Nijhof, The motion of a droplet subjected to linear shear flow including the presence of a plane wall, J. Fluid Mech. 302 (1995) 45–63.
[41] M.D. Chilcott, J.M. Rallison, Creeping flow of dilute polymer solutions past cylinders and spheres, J. Nonnewton Fluid Mech. 29 (1988) 381.
[42] H.M. Matos, M.A. Alves, P.J. Oliveira, New Formulation for Stress Calculation: application to Viscoelastic Flow in a T-Junction, Numerical Heat Transf., Part B: Fundamentals 56 (5) (2009) 351.

[43] G.N. Rocha, R.J. Poole, P.J. Oliveira, Bifurcation phenomena in viscoelastic flows through a symmetric 1:4 expansion, J. Nonnewton Fluid Mech. 141 (1) (2007) 1.
[44] P.J. Oliveira, A.l.I.P. Miranda, A numerical study of steady and unsteady viscoelastic flow past bounded cylinders, J. Nonnewton Fluid Mech. 127 (1) (2005) 51.
[45] M. Sahin, R.G. Owens, On the effects of viscoelasticity on two-dimensional vortex dynamics in the cylinder wake, J. Nonnewton Fluid Mech. 123 (2â€“3) (2004) 121.
[46] P.J. Coates, R.C. Armstrong, R.A. Brown, Calculation of steady-state viscoelastic flow through axisymmetric contractions with the EEME formulation, J. Nonnewton Fluid Mech. 42 (1â€“2) (1992) 141.
[47] K. Sarkar, W.R. Schowalter, Deformation of a two-dimensional viscoelastic drop at non-zero Reynolds number in time-periodic extensional flows, J Nonnewton Fluid Mech 95 (2–3) (2000) 315–342.
[48] S. Mukherjee, K. Sarkar, Lateral migration of a viscoelastic drop in a Newtonian fluid in a shear flow near a wall, Phys. Fluids 26 (2014), 103102.
[49] K. Sarkar, W.R. Schowalter, Deformation of a two-dimensional drop at non-zero Reynolds number in time-periodic extensional flows: numerical simulation, J. Fluid Mech. 436 (2001) 177–206.
[50] X.Y. Li, K. Sarkar, Drop deformation and breakup in a vortex at finite inertia, J. Fluid Mech. 564 (2006) 1–23.
[51] X. Li, K. Sarkar, Drop dynamics in an oscillating extensional flow at finite Reynolds numbers, Phys. fluids 17 (2) (2005), 027103.
[52] X.Y. Li, K. Sarkar, Numerical investigation of the rheology of a dilute emulsion of drops in an oscillating extensional flow, J Nonnewton Fluid Mech 128 (2–3) (2005) 71–82.
[53] P.O. Olapade, R.K. Singh, K. Sarkar, Pairwise interactions between deformable drops in free shear at finite inertia, Phys. Fluids 21 (6) (2009), 063302.
[54] R.K. Singh, K. Sarkar, Inertial effects on the dynamics, streamline topology and interfacial stresses due to a drop in shear, J. Fluid Mech. 683 (2011) 149–171.
[55] N. Aggarwal, K. Sarkar, Rheology of an emulsion of viscoelastic drops in steady shear, J. Nonnewton. Fluid Mech. 150 (1) (2008) 19–31.
[56] S. Mukherjee, K. Sarkar, Effects of viscosity ratio on deformation of a viscoelastic drop in a Newtonian matrix under steady shear, J. Nonnewton Fluid Mech. 160 (2–3) (2009) 104–112.
[57] S. Mukherjee, K. Sarkar, Effects of viscoelasticity on the retraction of a sheared drop, J. Nonnewton Fluid Mech. 165 (7–8) (2010) 340–349.
[58] S. Mukherjee, K. Sarkar, Viscoelastic drop falling through a viscous medium, Phys. Fluids 23 (1) (2011), 013101.
[59] W.S.J. Uijttewaal, E.J. Nijhof, R.M. Heethaar, Droplet migration, deformation, and orientation in the presence of a plane wall - a numerical study compared with analytical theories, Phys. Fluids a-Fluid Dynamics 5 (4) (1993) 819–825.
[60] M. Shapira, S. Haber, Low Reynolds number motion of a droplet in shear flow including wall effects, Int. J. Multiphase Flow 16 (2) (1990) 305.
[61] B.M. Lormand, R.J. Phillips, Sphere migration in oscillatory Couette flow of a viscoelastic fluid, J. Rheol. (N Y N Y) 48 (3) (2004) 551–570.
[62] S.D. Hudson, Wall migration and shear-induced diffusion of fluid droplets in emulsions, Phys. Fluids 15 (5) (2003) 1106–1113.
[63] M.R. King, D.T. Leighton, Measurement of shear-induced dispersion in a dilute emulsion, Phys. Fluids 13 (2) (2001) 397–406.
[64] J. Towns, et al., XSEDE: accelerating scientific discovery, Comp. Sci. Eng. 16 (5) (2014) 62–74.